Journal of Marine Research, 67, 411–433, 2009

Relative dispersion in the Nordic Seas

by I. Koszalka[1], J. H. LaCasce[1,2] and K. A. Orvik[3]

ABSTRACT

We examine the relative dispersion of surface drifters deployed in the POLEWARD experiment in the Nordic Seas during 2007–2008. The drifters were launched in pairs and triplets, yielding 67 pairs with an initial separation of 2 km or less. There were 26 additional pairs from drifters which subsequently came near one another. As these produced statistically identical dispersion to the original pairs, we used them as well, yielding 93 pairs.

The relative dispersion exhibits three phases. The first occurs during the first two days, at spatial scales less than 10 km. The dispersion increases approximately exponentially during this period, with an e-folding time of roughly half a day. During the second phase, from 2 to roughly 10 days and scales of 10 to roughly 100 km, the dispersion increases as a power law, with $r^2 \propto t^3$. At the largest spatial and temporal scales, the dispersion increases linearly in time and the pair velocities are uncorrelated, consistent with diffusive spreading.

We use a stochastic model with a representative mean flow to test the effect of the mean shear on dispersion. The model produces dispersion comparable to the observed during the second and third phases but fails to capture other statistics, such as the PDFs of the displacements. These statistics are instead suggestive of an inverse energy cascade, from the deformation scale up to 100 km.

1. Introduction

A cloud of tracer in a turbulent flow is both advected and strained. The advection can be quantified using single particle statistics (Davis, 1991). Straining, which reflects the spread about the cloud's center of mass, can be studied with pairs of particles (e.g. Bennett, 2006; LaCasce, 2008; Salazar and Collins, 2009). The study of pair ("relative") dispersion dates back to Richardson's (1926) seminal work in the atmospheric boundary layer. Relative dispersion is central to describing the spread of pollutants and the evolution of biological tracers. But it is also of theoretical value, as it can provide information about Eulerian statistics.

Many of our expectations about relative dispersion come from turbulence theory. Under certain conditions,[4] the relative dispersion can be used to deduce the Eulerian energy

1. Institute of Geosciences, University of Oslo, 1022 Blinden, 0315 Oslo, Norway.
2. Corresponding author. ***email: j.h.lacasce@geo.uio.no***
3. Geophysical Institute, University of Bergen, Allegt. 70, 5020 Bergen, Norway.
4. Specifically, if the flow is incompressible, homogeneous and statistically stationary.

spectrum (Kraichnan, 1966; Bennett, 1984). The relative dispersion (the mean square pair separation) is defined:

$$\langle r^2 \rangle = 1/N_p \sum_{i \neq j} (x_i - x_j)^2 + (y_i - y_j)^2, \tag{1}$$

where the sum is over all pairs of particles and N_p is the number of pairs. If the energy spectrum has a power law dependence:

$$E(k) \propto k^{-\alpha}, \tag{2}$$

with an exponent such that $1 < \alpha < 3$, the dispersion scales as:

$$\langle r^2 \rangle \propto t^{4/(3-\alpha)}. \tag{3}$$

This is known as *local dispersion*, because the dispersion is dominated by eddies comparable in size to the pair separation. The most familiar example is in the turbulent energy inertial range, for which $\alpha = 5/3$. Then the relative dispersion increases cubically in time, a relation known as Richardson's law.

If the spectrum is steeper, so that $\alpha > 3$, the dispersion is instead dominated by larger eddies. For such *non-local* dispersion, pair separations grow exponentially in time:

$$\langle r^2 \rangle \propto \exp\left(\frac{t}{\tau}\right) \tag{4}$$

where τ is a time scale related to the strain rate. This implies a sensitive dependence on initial conditions, because particles with slightly different positions separate exponentially.

If the pair separations are greater than the scale of the energy-containing eddies, the particles have uncorrelated velocities. Then relative dispersion is proportional to the single particle ("absolute") dispersion, with each particle behaving independently. The dispersion then increases linearly in time and the flow is "diffusive" because the diffusivity (the derivative of the dispersion) is constant (Taylor, 1921).

In the 1970s, pairs of balloons were launched near the tropopause in the Southern Hemisphere stratosphere in two large experiments: EOLE at 200 mb (Morel and Bandeen, 1973) and TWERLE at 150 mb (Jullian *et al.*, 1977). The relative dispersion was described by Morel and Larcheveque (1974) and Er-el and Peskin (1981), respectively. In both experiments there was evidence of exponential dispersion at scales less than roughly 1000 km, with an e-folding time on the order of one day. The dispersion at larger scales was less clear but indicated a power law dependence, with the dispersion increasing linearly in time or faster.

There have been few such relative dispersion experiments in the ocean. As such, relative dispersion has been studied using "chance pairs" consisting of instruments which happened to pass within a prescribed distance of each other at a certain time. LaCasce and Bower

(2000) used this technique with subsurface floats in the North Atlantic. Their results suggested the dispersion varies regionally; that in the eastern Atlantic is largely diffusive while Richardson-type growth occurs in the western Atlantic. The latter is likely connected with the Gulf Stream, which would explain why the dispersion differs in the east, which is more quiescent.

Ollitrault *et al.* (2005) examined a different set of subsurface floats, deployed in the mid-Atlantic. Many of these were deployed together so that the majority were actually original pairs. They also found indications for Richardson growth in the western Atlantic. But they also found the same type of growth in the eastern Atlantic.

In both studies, there were few pairs with separations smaller than the deformation radius. However, using a set of surface drifters in the Gulf of Mexico, LaCasce and Ohlmann (2003) obtained 140 chance pairs with an initial separation of 1 km, a scale substantially smaller than the local deformation radius (roughly 45 km). The dispersion at these scales appeared to be increasing exponentially in time, with an e-folding time scale on the order of a day.

But the small-scale dispersion remains controversial, both in the atmosphere and ocean. Using the "finite scale Lyapunov exponent" (FSLE; Aurell *et al*., 1997; Artale *et al.*, 1997) to re-examine the EOLE data, Lacorata *et al.* (2004) found clearer support for the Richardson law than exponential growth. Similarly, Lumpkin and Elipot (2010), who employed the FSLE with pairs of drifters launched in the Gulf Stream region, found the sub-deformation scale dispersion in the western Atlantic was closer to the Richardson law than an exponential.

Thus numerous questions remain concerning relative dispersion. Resolving the sub-deformation scales requires more pairs with small separations, and this demands experiments where the drifters or floats are launched together. Second, nearly all the aforementioned studies indicate Richardson dispersion at some scales. Okubo (1971) discovered this much earlier, in his analysis of tracer release experiments near the ocean surface. But the reason for Richardson dispersion remains obscure. This can occur under turbulent advection, as noted above, but can also stem from lateral shear advection (e.g. Bennett, 1987). Understanding this would help explain the discrepancy between the results in the eastern Atlantic between LaCasce and Bower (2000) and Ollitrault *et al.* (2005).

Hereafter we examine the relative dispersion of surface drifters deployed recently in the POLEWARD experiment in the Nordic Seas. In this, 118 drifters were deployed off the west coast of Norway in 2007 and 2008. The primary goal of POLEWARD was to study the Norwegian Atlantic Current (the northern branch of the North Atlantic Current) as it flows toward the Arctic Ocean. But a second goal was to measure relative dispersion. Thus the drifters were deployed in pairs and triplets.

The region is one of pronounced variability. The eddies generated by the Norwegian Atlantic Current spread several hundred kilometers offshore from the shelf break, with velocities of 50 cm/sec and more (e.g. LaCasce, 2005). These eddies play an important role in the thermohaline circulation, as they effectively increase the surface area of the warm inflow, prolonging the exposure to atmospheric cooling (Mauritzen, 1996). Relative dispersion here directly reflects the lateral mixing of these warm surface waters.

The paper is organized as follows. The data set is described in Section 2. In Part a, we compare the statistics of the original and chance pairs in the set. In Section 3, we examine how long and over what spatial scales the pair motion is correlated. The dispersion (Section 4) exhibits three regimes: one below the deformation radius, another up to scales of 50–100 km and the third at larger scales. In Sections 5 and 6 we examine possible causes for the intermediate scale dispersion.

2. Data

The POLEWARD data set consists of 118 surface drifters, of the type used in the Surface Velocity Program (SVP) of the World Ocean Circulation Experiment (WOCE) (e.g. Lumpkin and Pazos, 2007). Each drifter consists of a surface buoy, with a transmitter and a temperature sensor, and a subsurface drogue at 15-m depth. The drifter has a tether strain sensor, for monitoring the presence of the drogue. The drifters are tracked by the Argos satellite system, yielding positions with 150–1000 m accuracy up to 50 times a day.

The data were processed in two steps. First, zonal and meridional velocities were calculated by finite differencing the positions in time. A recursive de-spiking program was applied to remove velocities exceeding four standard deviations. We also eliminated positions for drifters which had lost their drogues or ceased to transmit reliably. We furthermore excluded segments from tracks near the ice edge, estimated by interpolating ice products (http://saf.met.no/p/ice/) onto individual trajectories. This affected 11 instruments. We then processed the data with a Butterworth filter with a 25-hour window, to suppress tidal and inertial motions, and re-sampled to 6 hour intervals.

We tested the effect of the filtering and de-spiking by recalculating the dispersion without either one. As might be expected, this altered the results at time scales less than a day, and significantly so only at times less than half a day. The dispersion without filtering is greater, presumably reflecting the effect of inertial motions.

We deployed a total of 27 pairs and 21 triplets. The latter were treated as yielding 3 pairs. The drifters were released along the path of the Norwegian Atlantic Current (Fig. 1) during 6 field campaigns from June, 2007, through October, 2008. Most (75 pairs) were deployed at the southern-most "Svinøy site." Additional drifters were deployed farther north, near the islands of Gimsøy (3 pairs) and Bjørnøy (3 pairs). One additional set of 3 pairs was deployed in the western Barents Sea. Four drifters failed to transmit or lost their drogue shortly after deployment, leaving 85 pairs.

The pairs and triplets were launched essentially simultaneously. As such, the initial separations, r_0, depend primarily on when the first satellite fix occurred. A histogram of the initial separations is shown in Figure 2a. There are 44 pairs with $r_0 \leq 1$ km, and 67 with $r_0 \leq 2$ km. However, we do not obtain many more pairs by using a larger r_0. As a trade-off then between having the smallest r_0 possible and the largest number of pairs, we choose $r_0 = 2$ km as our maximum initial separation.

As noted, pair mortality is affected by drogue life and environmental conditions. The number of pairs with $r_0 \leq 2$ km present as a function of elapsed time since deployment is

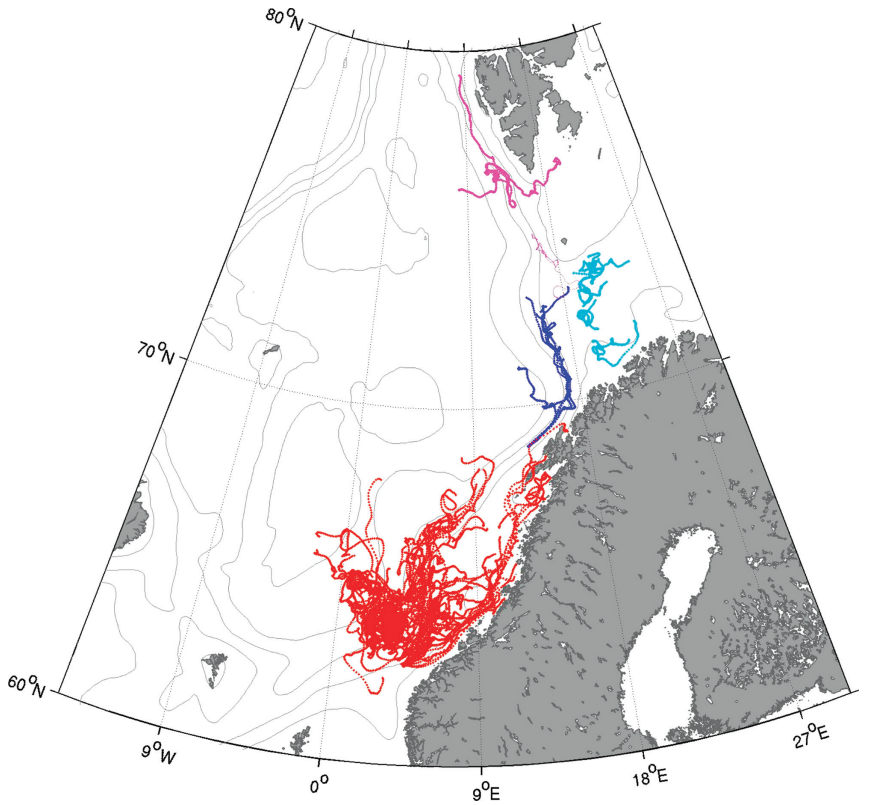

Figure 1. Drifter trajectories from the POLEWARD experiment during the first 40 days after deployment. The colors indicate deployment location: Svinøy (red), Gimsøy (blue), the Barents Sea (light blue) and Bjørnøy (magenta).

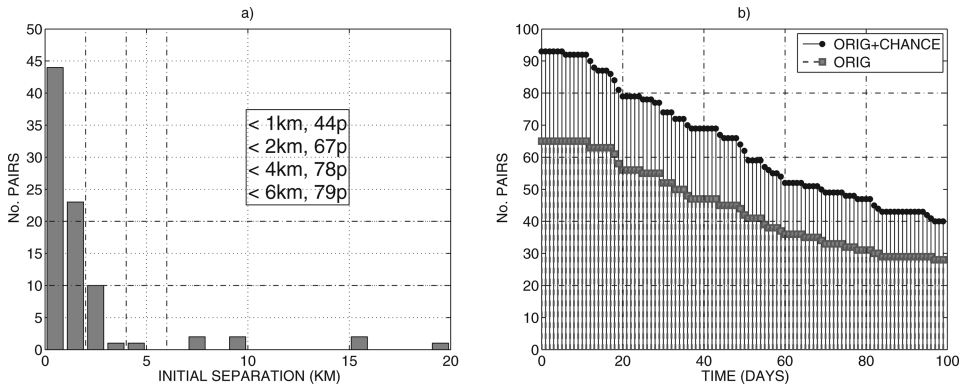

Figure 2. (a) Number of pairs vs. initial separation. (b) Number of pairs vs. elapsed time since deployment.

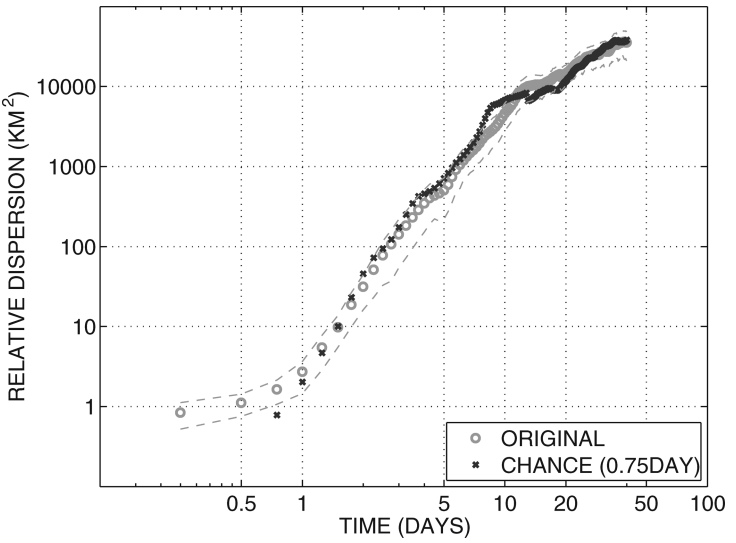

Figure 3. The relative dispersion for the original pairs and chance pairs. Both have $r_0 \leq 2$ km and the chance pair curve has been shifted by 0.75 days. The error bars, corresponding to the original pairs, are obtained by bootstrapping with 1000 samples.

shown in Figure 2b. The number decreases steadily in time, but there remain more than 40 pairs at 40 days. So our primary focus will be on this period.

This leaves 67 pairs with a maximum lifetime of 40 days. Of these, 59 were launched at Svinøy, 3 at Gimsøy, 2 at Bjørnøy and 3 in the Barents Sea. The drifters were also deployed at different locations relative to the bottom topography; 35 were deployed over the continental slope ($H < 1000$ m) and 32 in deeper water ($H < 1000$ m).

a. Chance pairs

As noted, several previous studies relied on "chance pairs," i.e., pairs of drifters not deployed together (Morel and Larcheveque, 1974; Er-el and Peskin, 1981; LaCasce and Bower, 2000; LaCasce and Ohlmann, 2003). This is potentially problematic because the initial pair separations may be correlated with the local velocities, and this can affect the subsequent dispersion (e.g. Babiano *et al.*, 1990). The POLEWARD drifters are "original pairs," so the correlation with the velocity should be less. However, the number of pairs (67 with $r_0 \leq 2$ km) is relatively small. We have 26 chance pairs with $r_0 \leq 2$ km, so including them would increase the sample size by 30%. But to do this, we must check their statistics in relation to those of the original pairs.

The relative dispersion from both pair types is compared in Figure 3. The error bars for the original pairs, calculated using a bootstrap method with 1000 subsamples, are also indicated. We see that the chance pair curve is not significantly different from the original

pair curve over the entire period. However, the chance pair curve must be shifted by 0.75 days to align with that for the original pairs. This suggests that there is an initial period, of the same duration, during which the original pairs adjust to the flow. Thereafter the chance pairs disperse like the original pairs.

A similar comparison was made with the EOLE balloons in the Southern Hemisphere stratosphere by Morel and Larcheveque (1974). Their conclusion was the same, that there was no statistical difference between chance and original pair dispersion. Thus, that study and the present finding lend credibility to the aforementioned analyses based on chance pairs.[5] Hereafter, we add the chance pairs to the original pairs, after shifting the former by 0.75 days. This yields a total of 93 pairs.

3. Correlated motion

A central point in interpreting pair dispersion is determining when the pair velocities are correlated. Turbulent dispersion implies correlated motion (Section 1), while random motion is associated with uncorrelated velocities. Here we use two different measures to establish how long and over what spatial scales the motion is correlated.

a. Relative velocity variance

The mean square separation velocity is defined:

$$\langle v^2(t)\rangle = 1/N_p \sum_{i\neq j} (u_i(t) - u_j(t))^2 = 2v^2 - 2\overline{u_i u_j}. \tag{5}$$

where v is the mean single particle velocity and u_i and u_j are the individual velocities (Kraichnan, 1966; LaCasce, 2008). Thus the squared separation velocity is twice the squared single particle velocity if the individual velocities are uncorrelated. If the velocities are correlated, the squared separation velocity is less.

The mean square separation velocity is shown in Figure 4a. Initially this is much less than twice the squared single particle velocity, but it increases during the first 6–10 days. After day 10 the two are not different within the errors. The corresponding rms single particle velocity is 25 cm/sec.

To determine the correlated spatial scales, we plot the relative velocity against pair separation (Fig. 4b). We obtain this by averaging velocities for all pairs which have a separation in a specified range, e.g. from 10–20 km, at a given time. The chosen distance ranges have a geometric scale dependence:

$$d_n = \gamma d_{n-1} = \gamma^n d_0 \tag{6}$$

5. An exception however was noted by Haza *et al.* (2008), in a study of synthetic drifters in the Adriatic. In their case, the chance and original pairs spanned different parts of the domain, with the chance pairs occurring primarily in a boundary current. So the two sets produced different dispersion.

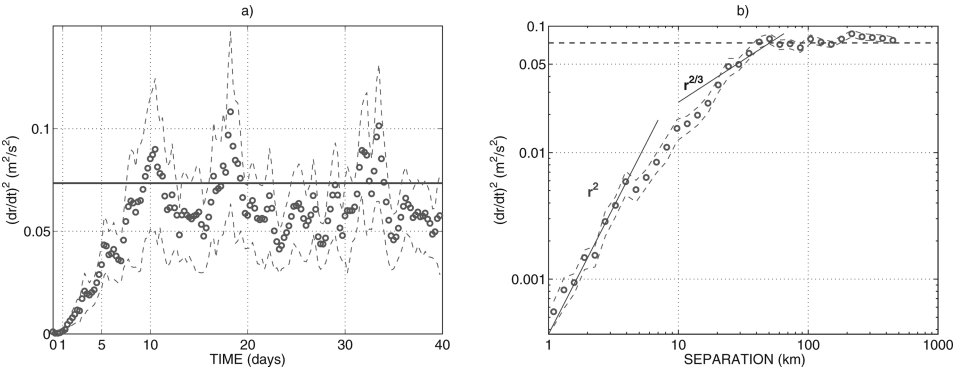

Figure 4. (a) Mean square separation velocity plotted vs. time since deployment, with errors from bootstrapping. (b) Mean square separation velocity plotted vs. time since deployment, with errors from bootstrapping. In both panels the solid line indicates twice the mean square single particle velocity, 0.053 m^2/sec^2.

which produces equally-spaced points on a logarithmic graph. For the scale factor, γ, we used a value of 1.2.

The results indicate the separation velocity increases over scales below 50–100 km. At larger scales, the value is near 0.07 m^2/sec^2, which is twice the squared single particle velocity (Fig. 4a). Thus the velocities at scales below 50–100 km are correlated. Also indicated in the figure are two power law regimes which occur at the smaller scales. These are discussed hereafter.

b. Separation angle

We can define another measure of correlated motion. This is based on the fact that the individuals in a correlated pair have nearly parallel velocity vectors. When they separate, the velocity vectors diverge. Consider the example in Figure 5a, which is representative. The colored bands on the individual trajectories indicate the number of days elapsed since deployment. During the first 4 days, the drifters move together, separating slowly. But on the fifth day, they veer apart, moving independently thereafter.

The angle between the velocity vectors is:

$$\theta = cos^{-1}\left(\frac{\vec{u}_1 \cdot \vec{u}_2}{|\vec{u}_1||\vec{u}_2|}\right). \tag{7}$$

The mean separation angle should indicate when the pairs are moving together, on average. Note that uncorrelated pairs will have a mean angle of 90 degrees, assuming a uniform distribution of angles between 0 and 180 degrees.

Shown in Figure 5b is the mean angle for all pairs with $r_0 \leq 2$ km. The average angle is near zero initially but increases thereafter, reaching 45 degrees by day 6. This is a typical

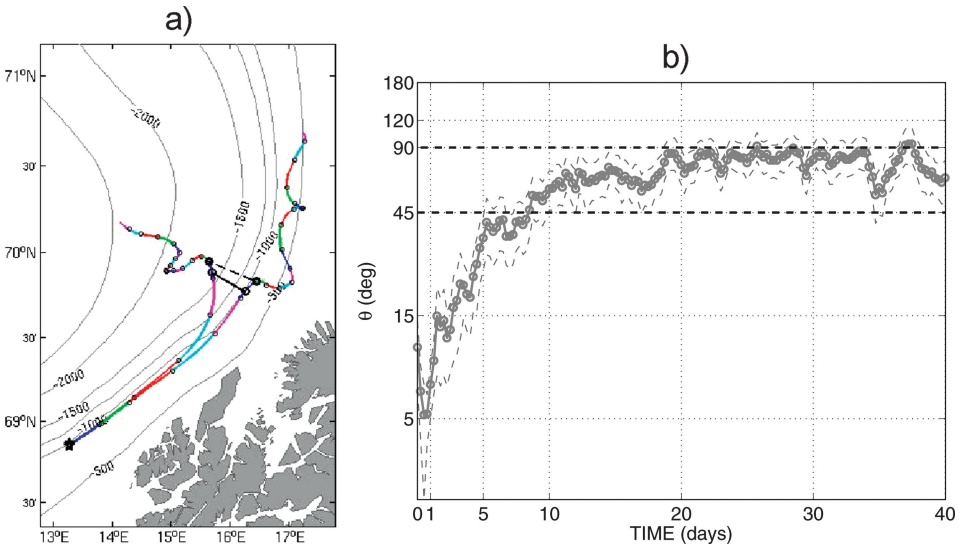

Figure 5. (a) Example of pair dispersion in the POLEWARD data set. The daily segments of drifter trajectories are color-coded. The dashed and solid lines indicate the times when the angle of separation θ is 45 and 90 degrees, respectively. (b) The mean separation angle between the individual velocities from the pairs with $r_o \leq 2$ km. The 95% confidence intervals are obtained by bootstrap re-sampling (1000 samples).

value when a pair is starting to split apart (e.g. Fig. 5a). By about 10 days, the mean angle is near 90 degrees. We conclude the first 6 days are correlated and that by 10 days most pairs are decorrelated, consistent with the conclusions based on the relative velocities.

Plotting the mean angle vs. pair separation (not shown) suggests that the angle is less than 45 degrees below about 30–50 km, and approaches 90 degrees at scales greater than 100 km. So the correlated spatial scales are also consistent with those inferred from the relative velocities.

Thus these two measures suggest the pair motion is correlated during roughly the first 10 days, up to 100 km in scale. The larger scales, and longer times, should correspond to single particle dispersion.

4. Relative dispersion

We now examine the relative dispersion in more detail. As noted, we focus on the first 40 days, as the number of pairs falls off thereafter.

Shown in Figure 6a is the total (zonal plus meridional) dispersion, plotted on a logarithmic graph, with error bars from bootstrapping. The figure suggests there are *three* distinct growth phases: one during the first two days, a second from 2 to roughly 10 days and a third thereafter. The intermediate and late phases exhibit power law dependencies on time, so that:

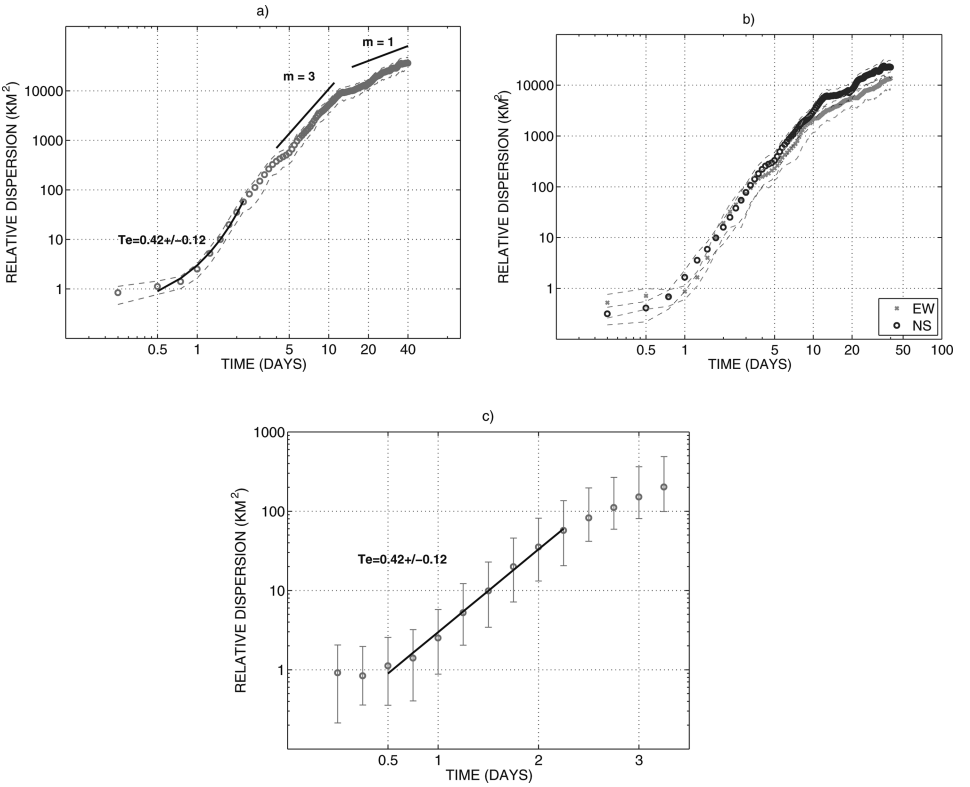

Figure 6. (a) Relative dispersion on a logarithmic graph. (b) The zonal and meridional dispersion. (c) The initial relative dispersion, on a semi-logarithmic graph; 95% confidence intervals are obtained by bootstrap re-sampling (1000 samples).

$$\langle r^2 \rangle \propto t^n \tag{8}$$

where r is the total separation. The exponents, determined by least squares, are $n = 2.9 \pm 0.2$ and $n = 1.2 \pm 0.3$, respectively. The growth in the early phase on the other hand is closer to exponential, with an e-folding time of roughly half a day.

The meridional and zonal dispersion are plotted separately in Figure 6b. During the initial and intermediate periods, the curves are not statistically different, indicating the dispersion is isotropic. During the late period, the meridional dispersion is somewhat greater than the zonal. Visual inspection of the trajectories confirms a slightly increased tendency for meridional dispersion at late times.

We also compared the dispersion for pairs deployed at the different sites and found the differences to be statistically insignificant. However, this is due in part to the fact that most of the pairs were deployed at Svinøy, so that the errors with the other subsets are larger. For instance, the Barents Sea dispersion is the weakest of the four groups, but there

are only 3 pairs there. There are some indications of a dependence on the water depth at deployment; pairs deployed in deep water disperse somewhat less than those over the slope. However, these differences are barely significant and do not persist. Thus we will assume the dispersion is approximately homogeneous and group all the pairs together when calculating the statistics.

In the following sections, we look more closely at each of the growth phases.

a. Initial phase

The initial phase pertains to the first two days and scales less than 10 km. In Figure 6c we plot the dispersion on a semi-logarithmic graph. The dispersion increases rapidly during this period, by roughly two orders of magnitude. Although the errors are large, the curve can be fit with an exponential over the period of 0.25 to 2.25 days. The e-folding time from least squares is $0.42 \pm .12$ days.

As noted in Section 1, exponential relative dispersion is characteristic of non-local dispersion, when the dispersion is dominated by eddies with scales larger than the pair separations. So, for instance, pairs with 1 km separations are advected by 10 km (or larger) eddies.

Non-local dispersion has specific implications for other statistics, and we can check those for consistency. With exponentially growing dispersion, the relative diffusivity scales as:

$$K = \frac{1}{2}\frac{d}{dt}\langle r^2 \rangle \propto r^2. \tag{9}$$

This is shown in Figure 7, plotted against separation distance. As with the relative velocities (Fig. 4b), we average in bins of geometrically increasing size. The diffusivity during the initial phase increases rapidly during the first three days, and the dependence is not different from r^2. However as the range is short, a definitive identification is not possible. One could argue that the quadratic dependence persists only to 5 km, or that a different dependence is also possible, given the errors. Nevertheless, the dependence is not inconsistent with non-local dispersion.

Non-local dispersion also has implications for the relative velocity. For one, the mean square relative velocity should scale as:

$$\langle (u_i - u_j)^2 \rangle \propto r^2 \tag{10}$$

(e.g. Morel and Larcheveque, 1974). The mean square relative velocity is shown in Figure 4b. As with the diffusivity the result is not indisputable, but the dependence is at least consistent with a quadratic dependence on r in this distance range.

In addition, non-local dispersion produces relative displacement distributions (PDFs) which have increasingly long tails (Lundgren, 1981; Bennett, 1984). This is because pairs

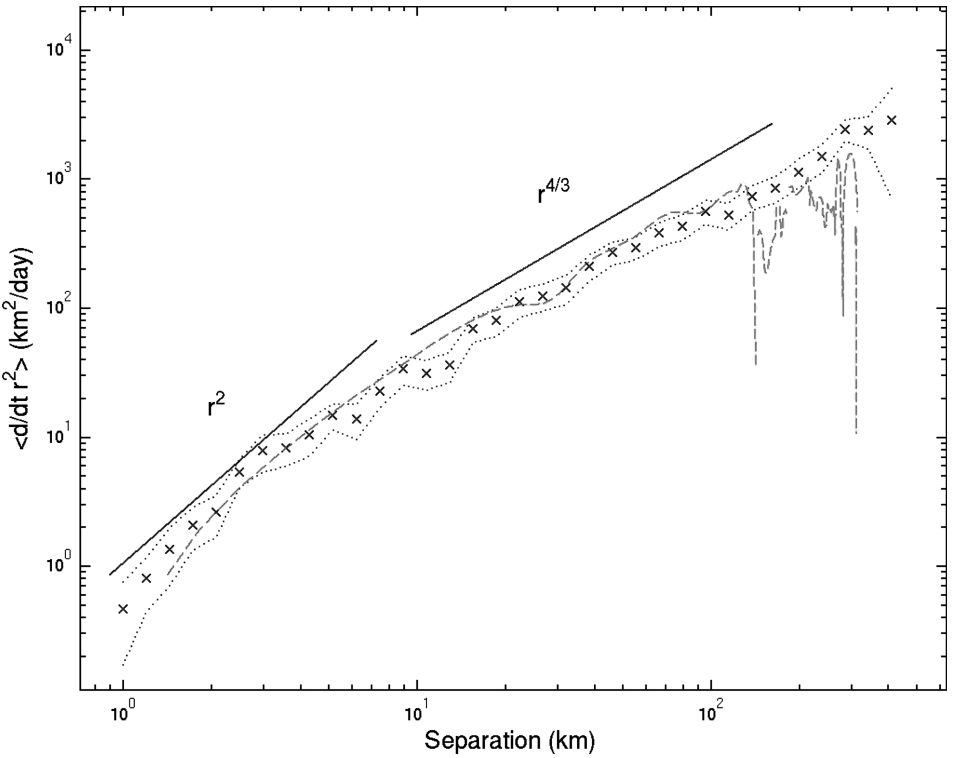

Figure 7. Relative diffusivity plotted against separation. The x's indicate the diffusivity obtained by averaging the instantaneous diffusivity by distance, and the dotted lines are the errors obtained from bootstrapping. The dashed line is the diffusivity from differencing the dispersion, plotted against the square root of the dispersion.

in rapidly straining regions separate much faster than other pairs. A way to detect this is with the displacement kurtosis, defined:

$$Ku \equiv \frac{\langle r^4 \rangle}{(\langle r^2 \rangle)^2} \tag{11}$$

(LaCasce and Bower, 2000; LaCasce and Ohlmann, 2003).[6] With exponential growth, the kurtosis should increase exponentially in time (Bennett, 1984).

The kurtosis over the first 40 days is plotted in Figure 8. For reference, we compare the result to the value obtained for a Rayleigh distribution (which is what one expects for a normally-distributed random process). A Rayleigh distribution has:

6. We define the kurtosis in terms of the raw moments, without the mean removed. We do this because the displacements are positive definite quantities. But the choice does not affect the results.

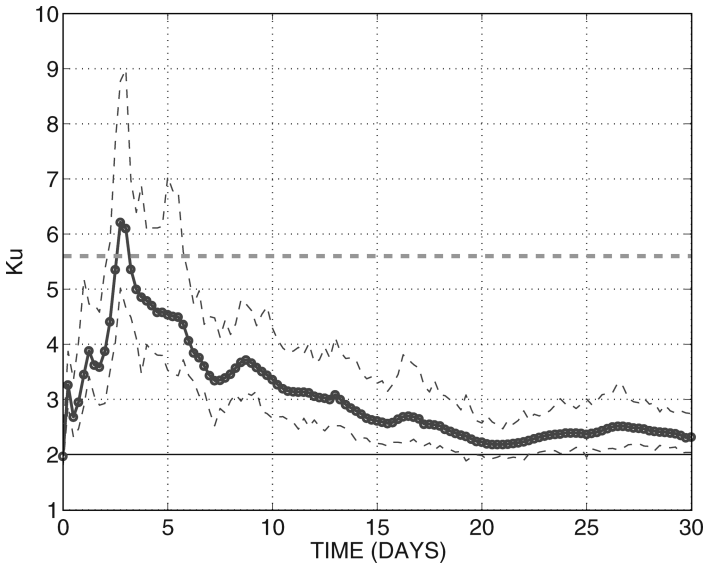

Figure 8. Displacement kurtosis as a function of time for the $r_0 \leq 2$ km pairs. The errors from bootstrapping, with 1000 subsamples, are indicated. The horizontal dashed and solid lines show the kurtosis for the Richardson and Rayleigh distributions.

$$p(r) = \frac{r}{\sigma^2} \exp\left(-\frac{r^2}{2\sigma^2}\right) \tag{12}$$

where σ is the variance. For a Rayleigh distribution, the kurtosis can be shown to be:

$$Ku = \frac{\Gamma(3)}{[\Gamma(2)]^2} = 2 \tag{13}$$

where Γ is the gamma function. We also calculated the conventional kurtosis (with the mean removed) and this produces similar results.[7]

The kurtosis increases rapidly during the first 2.5 days, from an initial value near 2 to a value near 6 (Fig. 8). It then decreases over the next 10 days, asymptoting to a value between 2 and 3. It is not possible to say whether the initial increase is exponential or not, due to the errors and short duration of the growth, but such growth is plausible.

Thus several measures are indicative of non-local dispersion during the initial period. Because 10 km is comparable to the local deformation radius, these results support exponential growth below that scale. However, due to the brevity of the initial period, a definitive identification of non-local dispersion is probably not possible.

7. LaCasce and Bower (2000) and LaCasce and Ohlmann (2003) used the kurtosis based on the de-meaned displacements. For a Rayleigh distribution, this has a value of 3.2451.

b. Intermediate phase

The intermediate phase occurs during the period 2–10 days, over scales of 10–100 km. The dispersion is consistent with:

$$\langle r^2 \rangle \propto t^3, \tag{14}$$

within the errors. This is as expected for a Richardson regime (Section 1). Under Richardson dispersion, the relative diffusivity should scale as:

$$K = \frac{1}{2}\frac{d}{dt}\langle r^2 \rangle \propto r^{4/3}. \tag{15}$$

The results in Figure 7 are consistent with such a growth in the intermediate range.

In addition, under local dispersion the displacement PDF is self-similar (it preserves its shape). Thus the kurtosis has a constant value. One can show that this value is 5.6 (LaCasce, 2009). We see instead that the kurtosis is falling during this period, reaching a value between 3 and 4 by day 10. This change in part reflects the relaxation which occurs from the very peaked PDF which develops during the initial period. But the PDF at the end of the intermediate period is less peaked than expected for a Richardson distribution.

Thus the results for the intermediate phase are mostly consistent with local dispersion, despite that the displacement PDF is evolving in time. As discussed in Section 1, identifying the *reason* for this dispersion is less simple. We consider two possibilities in Sections 5 and 6 hereafter.

c. Final phase

The logarithmic slope in the third phase is not significantly different from one, so that:

$$\langle r^2 \rangle \propto t. \tag{16}$$

This implies that the relative diffusivity is constant. Note though that the diffusivity calculated with respect to separation distance (Fig. 7) does not level off at large scales.[8] Thus the relative dispersion and distance-averaged diffusivity are at odds here.

The reason for this stems from the averaging process. The dispersion samples *all pairs* present at the late times, those with small and large separations. But the distance-averaged diffusivity at large scales represents only pairs with large separations. In the POLEWARD set, such pairs often have one member caught in the boundary current and the other in the interior. Such pairs have a distinctly rapid separation which is determined by the boundary current, not by random motion.

An alternate approach is to calculate the diffusivity from the derivative of the dispersion and plot the result against the square root of the dispersion (e.g. LaCasce and Bower, 2000).

8. A similar discrepancy was shown, but not noted, by Morel and Larcheveque (1974).

In this case, the dependent variable is the root mean square displacement, rather than the displacement itself. Calculated in this way, the diffusivity (the dashed line in Fig. 7) ceases to increase at scales greater than roughly 100 km. So by averaging all pairs present at late times, the diffusivity appears approximately constant at large scales.

In addition, the mean square relative velocities during the third phase are comparable to twice the mean square single particle velocity (Fig. 4a) and the kurtosis (Fig. 8) is similar to that for a Rayleigh distribution. Both observations suggest the final period is one of random motion, with the individuals in the pairs moving independently.

5. Stochastic model

There are several possible explanations for the Richardson dispersion seen in the intermediate period. As noted, this can occur under a turbulent energy cascade, but also with random motion in the presence of a mean shear. The Norwegian Atlantic Current dominates the flow in the region and has significant lateral shear, on the order of 0.3 f. The current has a north-south orientation as well, which could explain the meridional anisotropy seen in Figure 6b.

To test the current's effect, we examined the dispersion of synthetic particles in a representative mean flow. To do this, we used a first-order stochastic model (e.g. Griffa *et al.*, 1995; LaCasce, 2000; Veneziani *et al.*, 2004). In this, the particles have velocities determined by:

$$dx_i = (u_i + U(x, y))\, dt, \quad dy_i = (v_i + V(x, y))\, dt$$
$$du_i = -\frac{1}{T_L} u_i\, dt + \sqrt{\frac{2}{T_L}}\, v\, dw, \quad dv_i = -\frac{1}{T_L} v_i\, dt + \sqrt{\frac{2}{T_L}}\, v\, dw. \tag{17}$$

Here the subscript refers to the particle, (U, V) is the background mean flow and dw is a Wiener (normal) noise process. The velocity has two components, a "memory" of its previous value and a random noise component (representing eddy advection). The velocity autocorrelation decays as an exponential in this model with an e-folding time of T_L. The first order model is fairly realistic for simulating surface drifter motion (e.g. Griffa *et al.*, 1995; Veneziani *et al.*, 2004). The important point in the present context is that the stochastic drifters move independently at all times. So the results will be useful in determining the role of correlated velocities with the actual drifters.

We used three separate estimates of the mean field, (U, V):

- Geostrophic velocities derived from mean sea-surface height from the Rio and Hernandez (2004) climatology
- Mean velocities from a one year (2008–2009) simulation with the MIPOM model of the Norwegian Meteorological Institute (LaCasce and Engedahl, 2005 and refs. therein)
- Mean velocities obtained by averaging the drifter velocities in geographical bins.

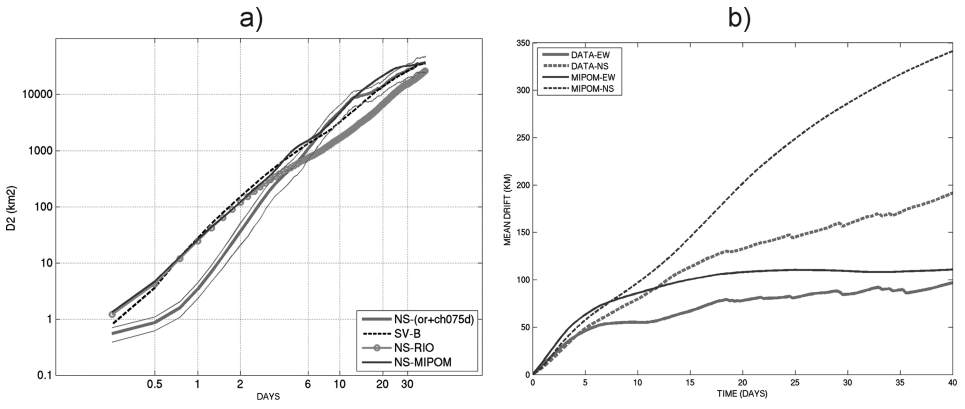

Figure 9. (a) Relative dispersion of the stochastic particles generated with various mean flows (sec. 5) compared to that of the POLEWARD drifters. (b) Mean single particle displacements for the POLEWARD data and the stochastic model with the MIPOM mean velocities.

Both the Rio and Hernandez and the binned drifter velocities have a resolution of 1/4 degree, which is coarser than the deformation scale of 10 km. The MIPOM mean has 4 km resolution and moreover exhibits fairly realistic structure, despite that its velocities are somewhat too weak (LaCasce and Engedahl, 2005). The Rio means pertain specifically to the surface while the MIPOM means correspond to a depth of 5 m.[9] The binned velocities were only calculated in the Svinøy region, where the drifter density is highest.

We deployed stochastic particles where the actual drifters were deployed, but used 10 times as many. When using the binned velocities, we deployed particles only at Svinøy. We use an integral time, T_L, of one day, based on estimates derived from the single particle velocity autocorrelation. A one-day time scale is also consistent with the expectation from the Eulerian integral time scale, which is of order 1–2 days (LaCasce, 2005). We then varied the noise amplitude, to produce a relative dispersion comparable in magnitude with the observed. Realistic dispersion was obtained with a noise amplitude of roughly 0.05 m/sec. This is smaller than the rms drifter velocity of 0.25 m/sec, but the latter represents the combination of mean and eddy advection.

The dispersion is shown in Figure 9a. All three stochastic curves exhibit an initial growth which is significantly faster than observed. This is to be expected, because the initial dispersion increases quadratically in time in the stochastic model, not exponentially. However, after roughly four days all three stochastic runs produce dispersion similar to the observed. The exception is the run with the RIO means which exhibits too weak dispersion. The other two runs yield reasonable dispersion during *both* the intermediate and late periods.

This suggests that the intermediate and late phases could be attributed to stochastic shear dispersion. The increased dispersion in the intermediate phase occurs when many of the

9. We use 5 m rather than 15 m because the model velocities at 5 m are stronger than, but also parallel to, those at 15 m, and thus more representative of the actual velocities at 15 m.

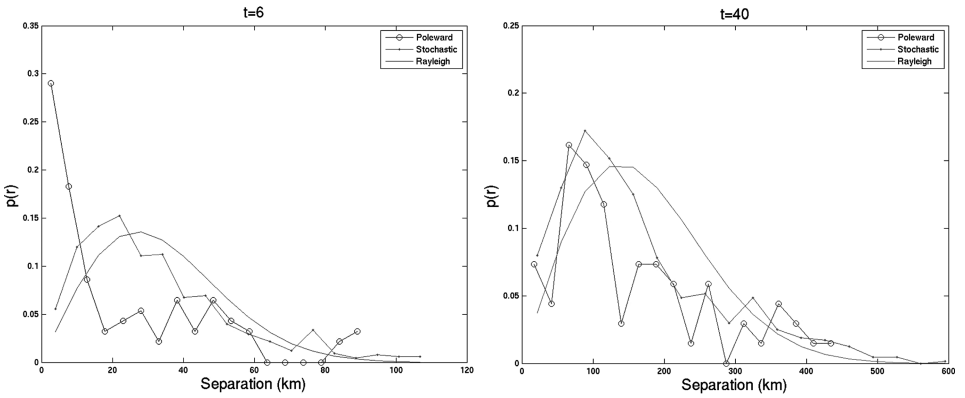

Figure 10. Relative displacement PDFs on (a) day 6 and (b) day 40 for the the POLEWARD drifter and the stochastic model with the MIPOM mean velocities. The PDFs have been normalized so that the sum of probabilities is one.

particles are near the cores of the mean flow, where the shear is greatest. At late times, the dispersion is less because the particles have exited the cores and are moving in regions with weaker background flow.

However, other measures suggest the intermediate phase cannot be attributed to shear dispersion. Consider for example the mean single particle displacement, shown in Figure 9b for the MIPOM mean field. The stochastic particles exhibit significantly greater mean drift, particularly in the meridional direction. This reflects that the stochastic particles follow the mean current to a greater degree than the actual drifters. This discrepancy is reduced if the noise amplitude is increased, as more particles then exit the mean flow; but then the model produces unrealistically large dispersion.

Then there are the probability density functions (PDFs) of the relative displacements. The PDFs at day 6 are compared in Figure 10a. The PDF for the stochastic particles is very near a Rayleigh distribution, consistent with random motion. But the observed PDF differs markedly, having many more small displacements and extended wings. The drifter kurtosis at day 6 is 3.5 (Fig. 8), only slightly larger than 2, but the PDF nevertheless differs markedly from a Rayleigh distribution.

The agreement with the stochastic model is better however during the late phase. The relative velocities indicate the individual velocities are decorrelated during this period. And the PDFs are in reasonable agreement as well. These are shown in Figure 10b, calculated from the displacements at day 40. Both the stochastic and actual drifters exhibit distributions which are comparable to the Rayleigh distribution.

So while the stochastic model can produce dispersion like that observed and appears to capture the late behavior, it cannot reproduce all the statistics during the intermediate phase. So we must turn to another explanation for this period.

6. Inverse cascade

Another possibility is that there is an energy cascade from the deformation scale (10 km) up to the 50–100 km scale. This could occur if deformation scale eddies, produced by the instability of the mean jets, were merging to produce larger eddies.

There is visual evidence of such eddies. In the offshore deployments in the Svinøy region, a subset of 20 drifters were caught up in coherent eddies (i.e., exhibited persistent, approximately circular motion). These eddies had scales exceeding 50 km, considerably larger than the deformation scale. A number of similar events, involving single drifters, were seen in the other regions as well.

Several statistical measures are also consistent with a cascade. If the turbulence is homogeneous, the mean square separation velocity is equivalent to the second order Eulerian structure function for the longitudinal velocities, defined:

$$\langle (u_l(\vec{x} + D, t) - u_l(\vec{x}, t))^2 \rangle. \tag{18}$$

Here the brackets indicate a spatial average and D is the separation between observations. In a two-dimensional energy cascade, the second order structure function scales as the separation, r, to the 2/3 power (Babiano *et al.*, 1985; Lindborg, 1999). The relative velocity plotted against distance Figure 4b does not yield a definitive power slope in the intermediate range, but a $r^{2/3}$ dependence is at least plausible.

Similarly, the *third* order structure function should increase linearly with separation in an energy cascade (e.g. Lindborg, 1999). The corresponding result in 3-D turbulence is Kolmogorov's "4/5 Law" (Frisch, 1995). The mean of the third power of the separation velocity is plotted in Figure 11 and this does exhibit a linear dependence on separation in the intermediate range. The inferred constant of proportionality is also positive, which is consistent with a negative flux of energy (a flux to larger scales). Note too that the third order moment increases as separation cubed at the small scales, which is as expected under non-local dispersion.

Taken together, these results are at least consistent with an inverse cascade in the region. This appears to be a more likely explanation for the behavior in the intermediate range than shear dispersion.

7. Summary and discussion

We have examined the relative dispersion of 118 surface drifters deployed in the POLEWARD experiment in the Nordic Seas during 2007–2008. The drifters were launched in pairs and triplets, yielding 67 pairs with an initial separation, r_0, of 2 km or less. We found 26 additional pairs from drifters which subsequently came near one another. These produce dispersion statistically identical to that of the original pairs, so we used them as well, yielding 93 pairs.

The relative dispersion occurs in three phases. The first occurs during the first two days, at spatial scales less than 10 km. The dispersion increases approximately exponentially during

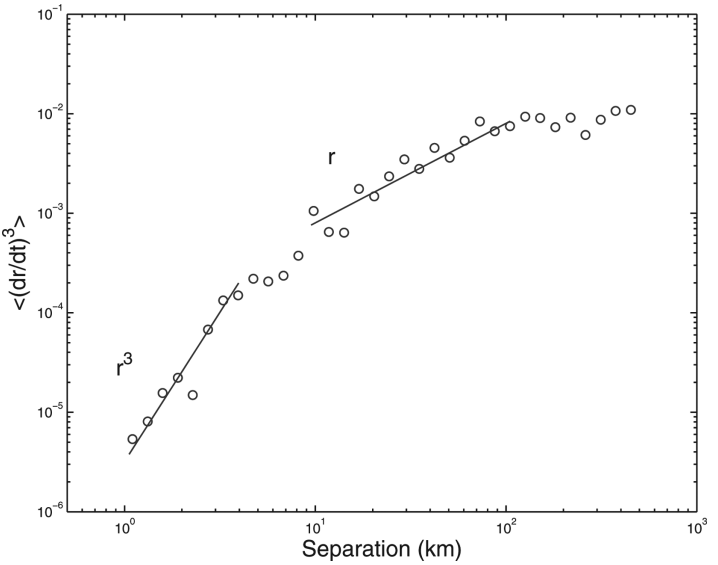

Figure 11. Third order structure function of the separation velocity as a function of separation.

this time, with an e-folding time near one half a day. Several other statistical measures, including the diffusivity, the displacement kurtosis and the third moment of the relative velocity, are also consistent with exponential growth.

During the second phase, from roughly 2–10 days and scales of 10–100 km, the dispersion increases as a power law, with $r^2 \propto t^3$. We found that a stochastic model with a representative mean flow could produce comparable dispersion. However, the stochastic model differs with other measures, such as the mean single particle drift and relative displacement distributions. The latter, and the relative velocity correlations, appear instead to be consistent with an inverse energy cascade.

At the largest separations, the dispersion increases linearly in time and the pair velocities are uncorrelated. Evidently, the drifters are dispersing diffusively at this point, in regions away from the cores of the mean flow.

The results are thus consistent with non-local relative dispersion at sub-deformation scales. Similar indications have been seen before in the stratosphere (Morel and Larcheveque, 1974; Er-El and Peskin, 1981), the surface ocean (LaCasce and Ohlmann, 2003) and in the subsurface ocean (Ollitrault *et al.*, 2005). However, the deformation radius in the Nordic Seas is small, so only one decade of scales is resolved in the data. A more definitive association, at least in this region, would require sampling with higher spatial resolution, e.g. with GPS tracking. But then the issue of dispersion by inertial motions would have to be addressed.

We also observe Richardson dispersion. LaCasce and Bower (2000) and Ollitrault *et al.* (2005) saw the same in the subsurface Atlantic, and LaCasce and Ohlmann (2003) and

Lumpkin and Elipot (2010) found evidence for this at the surface in the Atlantic. The present study is the first to rule out shear dispersion, i.e., random motion in the presence of the observed background shear, as a cause for this. It remains to be seen whether shear dispersion can be similarly discounted in the other cases.[10] If the dispersion is related to an inverse energy cascade, these results are in line those of with Scott and Wang (2005), who inferred and inverse cascade at the surface in the South Pacific from altimetric data.

We have focused primarily on the relative dispersion, the relative diffusivity and the displacement PDF. We have not discussed the finite scale Lyapunov exponent (FSLE), a measure favored in several recent studies. We did calculate the FSLE, but found the results weren't always straightforward to interpret. We believe this is due in part to the measure itself. As discussed by Lumpkin and Elipot (2010), using the FSLE requires subjective decisions. If, for example, a given pair separation exceeds 10 km and then decreases, does one count the time to the first crossing, the second crossing or both?

For this reason, we prefer the distance-averaged diffusivity, which is essentially the measure used by Richardson (1926). Like the FSLE, this involves averaging by distance and so differs fundamentally from the time-based relative dispersion. But it derives from the *instantaneous* diffusivity and so does not require such subjective choices. One shortcoming we observed with the measure is that the behavior at large scales may be biased by flow inhomogeneities, specifically large-scale coherent flows. A similar effect should affect the FSLE, since it is also based on distance averages. This effect might explain discrepancies seen before between relative dispersion and the FSLE at large separations (LaCasce and Bower, 2000; LaCasce and Ohlmann, 2003; Lumpkin and Elipot, 2010).

Recently, several authors have argued that the surface ocean may be dominated by *surface quasi-geostrophic* (SQG) dynamics (Lapeyre and Klein, 2006; LaCasce and Mahadevan, 2006; Isern-Fontanet *et al.*, 2006; Capet *et al.*, 2008; Lumpkin and Elipot, 2010). SQG turbulence can produce an energy cascade like that in two dimensions, with a spectral slope of $k^{-5/3}$. Such a slope is observed in the upper troposphere, below scales of 500–1000 km, and this has been interpreted as a sign of SQG turbulence on the tropopause (Tulloch and Smith, 2006). At larger scales, there is clear evidence of a k^{-3} spectrum (Nastrom and Gage, 1985), consistent with a 2-D enstrophy cascade (Charney, 1971).

Interestingly, the present observations are the opposite. We infer a $k^{-5/3}$ spectrum (an energy cascade) at intermediate scales, above the deformation radius, and a k^{-3} (or steeper) spectrum below the deformation radius. This is more in line with the traditional paradigm of geostrophic turbulence in the presence of baroclinic instability (Salmon, 1980). So we infer that SQG may not be relevant in this region.

We have not discussed surface divergence effects. Indeed, it is not obvious that 2-D turbulence is a relevant paradigm at the surface as that theory applies to non-divergent

10. Ollitrault *et al.* (2005) suggested shear dispersion was an unlikely culprit in their study as the dispersion was isotropic over the relevant scales. But their displacement PDFs resembled the Rayleigh distribution over the same scales, suggesting random motion.

fluids. Davis (1985) did not find a systematic dependence of diffusivity on distance at the surface in the California Current and suggested this might have been due to divergences.

We do see obvious evidence for divergence effects. Numerical studies of particles confined to a 2-D surface in the presence of 3-D turbulence exhibit particle clustering along lines (Schumacher and Eckhardt, 2002), similar to the clustering of debris between surface Langmuir cells. We did not find instances of such clustering in any of the locations.

As suggested by LaCasce and Ohlmann (2003), this could be because the surface velocities are nearly geostrophic. Then the flow would be horizontally non-divergent at first order and vertical velocities an order of magnitude smaller. Nevertheless, divergence effects deserve more attention, both in numerical models and in experiments in which relative dispersion is simultaneously measured at the surface and sub-surface.

Acknowledgments. The work is part of the Poleward project, funded by by the Norwegian Research Council Norklima program (grant number 178559/S30). Details are found on http://www.iaoos.no/. The data were processed at AOML by Mayra Pazos and co-workers (http://www.aoml.noaa.gov/phod/dac/gdp.html). Harald Engedahl provided the MIPOM velocities. JHL had useful discussions with A. Bennett about PDFs and R. Lumpkin kindly sent us a copy of his manuscript. We also received useful comments from two anonymous reviewers.

REFERENCES

Artale, V., G. Boffetta, A. Celani, M. Cencini and A. Vulpiani. 1997. Dispersion of passive tracers in closed basins: beyond the diffusion coefficient. Phys. Fluids, *9*, 3162–3171.

Aurell, E., G. Boffetta, A. Crisianti, G. Paladin and A. Vulpiani. 1997. Predictability in the large: an extension of the concept of Lyapunov exponent. J. Physics A: Mathematical General, *30*, 1–26.

Babiano, A., C. Basdevant, P. LeRoy and R. Sadourny. 1990. Relative dispersion in two-dimensional turbulence. J. Fluid Mech., *214*, 535–557.

Babiano, A., C. Basdevant and R. Sadourny. 1985. Structure functions and dispersion laws in two-dimensional turbulence. J. Atmos. Sci., *42*, 941–949.

Bennett, A. F. 1984. Relative dispersion: local and nonlocal dynamics. J. Atmos. Sci., *41*, 1881–1886.

—— 1987. A Lagrangian analysis of turbulent diffusion. Rev. Geophys., *25*, 799–822.

—— 2006. Lagrangian Fluid Dynamics, Cambridge University Press, 286 pp.

Capet, X., P. Klein, B. L. Hua, G. Lapeyre and J. C. McWilliams. 2008. Surface kinetic energy transfer in surface quasi-geostrophic flows. J. Fluid Mech., *604*, 165–174.

Charney, J. G. 1971. Geostrophic turbulence. J. Atmos. Sci., *28*, 1087–1093.

Davis, R. E. 1991. Observing the general circulation with floats. Deep-Sea Res., *38* (Suppl.), S531–S571.

Er-el, J. and R. Peskin. 1981. Relative diffusion of constant-level balloons in the Southern hemisphere. J. Atmos. Sci., *38*, 2264–2274.

Frisch, U. 1995. Turbulence, The Legacy of A.N. Kolmogorov, Cambridge Univ. Press, 296 pp.

Griffa, A., K. Owens, L. Piterbarg and B. Rozovskii. 1995. Estimates of turbulence parameters from Lagrangian data using a stochastic particle model. J. Mar. Res., *53*, 371–401.

Haza, A. C., A. C. Poje, T. M. Ozgokmen and P. Martin. 2008. Relative dispersion from a high-resolution coastal model of the Adriatic Sea. Ocean Model., *22*, 48–65.

Isern-Fontanet, J., B. Chapron, G. Lapeyre, and P. Klein. 2006. Potential use of microwave sea surface temperature for the estimation of oceanic currents. Geophys. Res. Lett., *33*, 11–15.

Jullian, P., W. Massman and N. Levanon. 1977. The TWERLE experiment. Bull. Am. Met. Soc., *58*, 936–948.

Kraichnan, R. H. 1966. Dispersion of particle pairs in homogeneous turbulence. Phys. Fluids, *9*, 1937–1943.

LaCasce, J. H. 2005. Statistics of low frequency currents over the western Nordic shelf and slope; part I, current meters. Ocean Dyn., *55*, 213–221.

—— 2008. Statistics from Lagrangian observations. Prog. Oceanogr., *77*, 1–29.

—— 2009. Relative dispersion PDFs in 2-D turbulence and in observations. (*in prep.*).

LaCasce, J. H. and A. Bower. 2000. Relative dispersion in the subsurface North Atlantic. J. Mar. Res., *58*, 863–894.

LaCasce, J. H. and H. Engedahl. 2005. Statistics of low frequency currents over the western Nordic shelf and slope; part II, model. Ocean Dyn., *55*, 222–237.

LaCasce, J. H. and A. Mahadevan. 2006. Estimating subsurface horizontal and vertical velocities from sea-surface temperature. J. Mar. Res., *64*, 695–721.

LaCasce, J. H. and C. Ohlmann. 2003. Relative dispersion at the surface of the Gulf of Mexico. J. Mar. Res., *61*, 285–312.

Lacorata, G., E. Aurell, B. Legras and A. Vulpiani. 2004. Evidence for a $\kappa^{-5/3}$ spectrum from the EOLE Lagrangian balloons in the low stratosphere. J. Atmos. Sci., *61*, 2936–2942.

Lapeyre G. and P. Klein. 2006. Dynamics of the upper oceanic layers in terms of surface quasi-geostrophic theory. J. Phys. Oceanogr., *36*, 165–176.

Lindborg, E. 1999. Can the atmospheric kinetic energy spectrum be explained by two-dimensional turbulence? J. Fluid Mech., *388*, 259–288.

Lumpkin, R. and S. Elipot. 2010. Surface drifter pair spreading in the North Atlantic. J. Geophys. Res. (submitted).

Lumpkin, R. and M. Pazos. 2007. Measuring surface currents with SVP drifters, in Lagrangian Analysis and Prediction of Coastal and Ocean Dynamics, a. Griffa *et al.*, eds., Cambridge University Press, 39–67.

Lundgren, T. S. 1981. Turbulent pair dispersion and scalar diffusion. J. Fluid Mech., *111*, 27–57.

Mauritzen, C. 1996. Production of dense overflow waters feeding the North Atlantic across the Greenland-Scotland Ridge. Part 1: evidence for a revised circulation scheme. Deep-Sea Res. I, *43*, 769–806.

Morel, P. and W. Bandeen. 1973. The EOLE experiment, early results and current objectives. Bull. Am. Met. Soc., *54*, 298–306.

Morel, P. and M. Larcheveque. 1974. Relative dispersion of constant-level balloons in the 200 mb general circulation. J. Atmos. Sci., *31*, 2189–2196.

Nastrom, G.D. and K.S. Gage. 1985. A climatology of atmospheric wavenumber spectra of wind and temperature observed by commercial aircraft. J. Atmos. Sci., *42*, 950–960.

Okubo, A. 1971. Oceanic diffusion diagrams. Deep-Sea Res., *18*, 789–802.

Ollitrault, M., Gabillet, C. and A. Colin de Verdiere. 2005. Open ocean regimes of relative dispersion. J. Fluid Mech., *533*, 381–407.

Richardson, L. F. 1926. Atmospheric diffusion on a distance-neighbour graph. Pro. Royal Soc. London, Series A, *110*, 709–737.

Rio, M.-H. and F. Hernandez. 2004. A mean dynamic topography computed over the world ocean from altimetry, *in situ* measurements and a geoid model. J. Geophys. Res., *109*, doi: 10.1029/2003JC002226.

Salazar, J. P. L. C. and L. R. Collins. 2009. Two-particle dispersion in isotropic turbulent flows. Ann. Rev. Fluid Mech., *41*, 405–432.

Salmon, R. 1980. Baroclinic instability and geostrophic turbulence. Geophys. Astrophys. Fluid Dyn., *10*, 25–52.

Schumacher, J. and B. Eckhardt. 2002. Clustering dynamics of Lagrangian tracers in free-surface flows. Phys. Rev. E, *66*, 017303.

Scott, R. B. and F. Wang. 2005. Direct evidence of an oceanic inverse kinetic energy cascade from satellite altimetry. J. Phys. Oceanogr., *35*, 1650–1666.

Taylor, G. I. 1921. Diffusion by continuous movements. Pro. London Math. Soc., *20*, 196–212.

Tulloch, R. and K. S. Smith. 2006. A theory of the atmospheric energy spectrum: Depth-limited temperature anomalies at the tropopause. Pro. Natl. Acad. Sci., *103*, 14690–14694.

Veneziani M., A. Griffa, A. M. Reynolds and A. J. Mariano. 2004. Oceanic turbulence and stochastic models from subsurface Lagrangian data for the North-West Atlantic Ocean. J. Phys. Oceanogr., *34*, 1884–1906.

Received: *4 May, 2009*; revised: *15 October, 2009*.